

Globular Clusters Formed within Dark Halos I: present-day abundance, distribution and kinematics

Peter Creasey^{1*}, Laura V. Sales¹, Eric W. Peng², and Omid Sameie^{1†}

¹ *Department of Physics and Astronomy, University of California, Riverside, California 92507, USA*

² *KIAA & Department of Astronomy, Peking University, Beijing 100871, China*

2 April 2022

ABSTRACT

We explore a scenario where metal poor globular clusters (GCs) form at the centres of their own dark matter halos in the early Universe before reionization. This hypothesis leads to predictions about the abundance, distribution and kinematics of GCs today that we explore using cosmological N-body simulations and analytical modelling. We find that selecting the massive tail of collapsed objects at $z \gtrsim 9$ as GCs formation sites leads to four main predictions: *i*) a highly clustered population of GCs around galaxies today, *ii*) a natural scaling between number of GCs and halo virial mass that follows roughly the observed trend *iii*) a very low number of free floating GCs outside massive halos and *iv*) GCs should be embedded within massive and extended dark matter (sub)halos. We find that the strongest constraint to the model is given by the combination of *i*) and *ii*): a mass cut to tagged GCs halos which accounts for the number density of metal poor GCs today predicts a radial distribution that is too extended compared to recent observations. On the other hand, a mass cut sufficient to match the observed half number radius could only explain 60% of the metal poor population. In all cases, observations favour early redshifts for GC formation ($z \geq 15$).

Key words: galaxies: formation - galaxies: evolution - galaxies: structure - cosmology: theory - methods: numerical

1 INTRODUCTION

Globular Clusters (GCs) are fundamental probes of star formation in the early Universe and offer a unique local window to the physics and conditions from the vantage of the evolved Universe. GCs harbour one of the most ancient stellar populations, with estimates for the upper limit in ages of Milky Way GCs of 13.4 ± 2.2 Gyr (Krauss & Chaboyer 2003). Although GCs present a wide range of ages and metallicities (Peng et al. 2006; Harris et al. 2015), it is interesting to consider that the older and more metal poor objects could have formed in the pre-reionization era, and furthermore, that their stars may have contributed to the total budget of photons that drove reionization (Griffen et al. 2013; Boylan-Kolchin 2017).

Despite their relevance to star formation, galaxy evolution and cosmology, there is no clear consensus on the formation of GCs. This stems in part from the large spread in observed GCs properties, likely suggesting that there is more than one formation mechanism in play. For instance, the metal rich population of GCs is believed to be formed

mostly in-situ from the inter-stellar-medium (ISM) of galaxies, with an efficiency higher in disks that are more gas rich, highly pressurised and turbulent (Kruijssen 2015), conditions that are more prevalent at high redshift, and would naturally explain the old ages inferred for GCs. This scenario is also supported by observations of nearby interacting galaxies that exhibit distinctive knots of young stellar associations that could be hypothesised to survive as self-bound GCs today, as well as studies of young stellar clusters in the MW and star forming galaxies (Goddard et al. 2010; Bastian et al. 2013; Adamo et al. 2015). In this fashion, metal rich GCs are born out of the ISM in galaxies that are later re-distributed into a more extended “halo” like configuration due to dynamical processes such as scattering by molecular clouds, mergers and galaxy interactions (Kravtsov & Gnedin 2005; Prieto & Gnedin 2008).

On the other hand, older and more metal poor GCs are consistent with being accreted from smaller galaxy satellites (van den Bergh 2000) as part of the cosmological assembly of halos. For instance, in the Milky Way (MW) several GCs have been associated to known stellar streams and dwarf galaxies (Cohen 2004; Law & Majewski 2010). Coherent rotation (which could be an indicator of coherent infall) has also been observed for M31 (Veljanoski et al. 2014), a sit-

* E-mail: peter.creasey@ucr.edu

† NASA MIRO FIELDS fellow

uation that has also been found in simulations (Veljanoski & Helmi 2016). Another plausible formation mechanism for GCs has been recently proposed by Naoz & Narayan (2014) where non-negligible streaming velocities between the gas and the dark matter at high redshifts might cause the baryonic collapse of GC-mass objects outside the virial radius of the dark matter halos. In a final alternative, metal poor GCs could represent the end product of galaxy formation on low mass dark matter halos (Peebles 1984). This scenario proposes that GCs form before reionization *at the centres of their own dark matter halos*, in a similar fashion to dwarf galaxies do, but extending the host halo mass regime towards lower virial masses, and to baryonic objects where DM halos have not been detected. Interestingly, high resolution hydrodynamical simulations of first galaxies are starting to support the formation of very compact stellar systems within early collapsed halos that are structurally similar to the population of GCs (Kimm et al. 2016; Ricotti et al. 2016a).

The idea of GCs inhabiting their own dark halos has been explored in the past with some attractive conclusions. Three shall be highlighted: radial distribution of GCs, the scaling between GCs content and virial mass of the halo and, most importantly, the fact that GCs will then be predicted to contain large fractions of dark matter. We discuss each of them individually below.

- *Radial distribution of GCs:* Selecting rare peaks of density fluctuation in the early Universe as sites of GC formation leads to a present-day distribution of GCs that is highly clustered around massive host halos such as MW mass and above (Diemand et al. 2005; Moore et al. 2006). Whether the distribution is clustered enough is a subject of study of the present paper. For instance, the radial profile of the MWs metal poor GCs has a median radius of 7.1 kpc (Harris 1996, (2010 edition) and decays with exponent $r^{-7/2}$ (Harris 1976). For comparison, the early work by Diemand et al. (2005) populating GCs in high density peaks has given a consistent radial distribution of GCs around a MW-like halo along with a relatively compact median radius of 17 kpc (which is significantly more extended than the aforementioned blue GCs population in the MW, although still far from the ≈ 90 kpc median radius of the total dark matter halo material).

Furthermore, more recent approaches to this problem have suggested that these compact distributions of GCs in the MW may be reconciled with predictions of this scenario by assuming a rather early reionization time, $z \leq 13$, for the MW region (Bekki 2005; Busha et al. 2010). Although earlier than the suggested reionization time by the latest Planck analysis, $z_{\text{re}} = 8.8^{+1.7}_{-1.4}$, (Planck Collaboration et al. 2016, from the Thompson scattering of CMB photons by free electrons), this may still be accommodated in a scenario where reionization is patchy (see e.g. Busha et al. 2010; Lunnan et al. 2012; Griffen et al. 2013) and was locally driven earlier either by the MW itself or by nearby massive structures such as the Virgo cluster (Iliev et al. 2011; Aubert et al. 2018). Encouragingly, the sizes of globular cluster distributions around external galaxies is beginning to become available for a large sample of galaxies (Lim et al., in prep.; Georgiev et al. 2010; Hudson & Robison 2017; Forbes 2017), providing strong constraints to this model.

- *GC abundance that scales with M_{vir} :* Due to the self-similarity of the Λ cold dark matter model (Λ CDM) and its

predicted level of substructure (Yang et al. 2011), a model where GCs form at high redshift dependent only upon halo mass sets up a relationship *today* where the total number or mass of GCs¹ is nearly linear in the halo mass (see also Boylan-Kolchin 2017), with recent estimates of the normalisation in observations of $M_{\text{GC}}/M_{\text{halo}}$ of around 4×10^{-5} (Hudson et al. 2014). Formation of such a trend from later-time baryonic processes is more difficult since in general the stellar distribution or galactic baryon distribution is highly nonlinear in halo mass (e.g. Moster et al. 2013), causing Blakeslee (1997) to memorably comment: “galaxies do not have too many globular clusters for their luminosity, they are underluminous for their number of globular clusters”. However, it seems that the linear scaling between GC mass and halo mass also arises naturally as consequence of the hierarchical nature of Λ CDM, even if they formed through fully baryonic processes, and therefore is a weak probe of GC formation scenarios (El-Badry et al. 2018).

- *Dark Matter content in GCs:* The most straightforward consequence this scenario is the implication that GCs should be surrounded by an extended and massive dark matter halo, in a similar fashion as inferred for dwarfs and more massive galaxies. Unfortunately the baryonic content of GCs is extremely compact with a scale radius of just a few parsecs, which in comparison to a dark halo with scale radius of a kpc (Conroy et al. 2011) implies that within the half light radii we expect the dark matter content to contribute just a few percent to the matter density, making the discrimination of its presence or absence a demanding task. Although stellar dynamics are not available in the dark-matter dominated regions of the outer halos, stellar light profiles and kinematics have been used to attempt a dynamical modelling able to constrain the matter content of some MW GCs (e.g. Lane et al. 2010; Conroy et al. 2011; Ibata et al. 2013; Peñarrubia et al. 2017) which have not found evidence for DM halos, albeit with the additional invocation of assumptions about levels of equilibrium/relaxation and tidal heating and stripping. Interestingly, high mass-to-light ratios have been detected in GCs outside the MW (Taylor et al. 2015), although the distribution seem so compact that is better explained by central black holes (Bovill et al. 2016) or some peculiar stellar population (T. Puzia, private communication) than by a surrounding dark matter halo.

Further interesting predictions from this simple model includes the dynamics of GCs (now dictated by cosmological infall of subhalos) and the existence of very few GCs expected to have survived until $z = 0$ in isolation, i.e. outside the virial radius of galaxies and clusters. Whereas promising new measurements from observations are starting to constrain the kinematics of GCs (Zhu et al. 2014; Deason et al. 2013; Napolitano et al. 2014; Spitler et al. 2012), the searches for ‘intergalactic’ GCs in the large SDSS data-set has not confirmed any candidates so far (di Tullio Zinn & Zinn 2015; Mackey et al. 2016). Therefore, as observational data starts to constrain the full space of predictions by the model, the jury is still out on whether primordial GCs could explain (or

¹ The relation with GC number (e.g. Zepf & Ashman 1993) appears to have more scatter than using GC stellar mass (Spitler & Forbes 2009).

partially explain) the population of metal poor GCs around galaxies.

Studying the formation of GCs in cosmological hydro simulations is extremely challenging given the large dynamical range needed to resolve the inner structure of GCs (pc-scale) together with the formation and environment of halos on Mpc-scales (Kravtsov & Gnedin 2005; Ricotti et al. 2016b; Mistani et al. 2016; Li et al. 2017; Kimm et al. 2016; Renaud et al. 2017; Pfeffer et al. 2018). We instead employ a complementary approach where N-body only cosmological simulations are used to identify the possible sites of formation of GCs and a ‘tagging’ criteria to follow the GC evolution (in a collisionless way) up to redshift $z = 0$. We explore the implications of GCs forming as the central objects in dark matter halos at the redshift of reionization with specific focus on the conditions required to satisfy observational constraints on abundance, radial distribution and the observed (or lack thereof) intergalactic globular cluster (IGC) distribution. We expand previous studies using a similar technique, by looking at the GC population predicted in a wide range of halo mass (M_{200} from 10^{11} - $10^{12.6} M_{\odot}$), instead of analysing the MW-like halos only. Finally we also consider the implication w.r.t. DM in the GCs *today*, and to what extent observations of the extended stellar halos (of GCs) can constrain this.

This paper is organised as follows. In Section 2 we describe our dark matter only numerical simulation that is large enough to capture several MW-like objects, yet high enough resolution to identify the progenitor halos that could be hosting GCs today, and how we tag our GCs. In Section 3 we make a comparison of this population to the observed GC population, with particular attention to the abundance of GCs and their radial distribution. In Section 4 we follow their orbital dynamics around their hosts and in Section 5 consider the abundance of external ‘intergalactic’ GCs. In Section 6 we summarise and conclude.

2 COSMOLOGICAL SIMULATION

In order to identify dark matter halos in Λ CDM that are numerous enough at redshift 10 to be the hosts for an old GC population one needs to resolve halos down to a mass of a few $\times 10^7 M_{\odot}$, and yet be large enough to contain several MW like objects (i.e. within a factor of a few of a halo mass of $10^{12} M_{\odot}$) implying one needs to simulate a volume of several hundreds of comoving Mpc^3 . Analytic models such as Press & Schechter (1974) can be used if one is only interested in the mass evolution and assembly history (e.g. as done for a similar GC formation scenario by Boylan-Kolchin 2017; El-Badry et al. 2018), yet if one needs the dynamics and the geometry one must turn to N-body simulation.

As such we choose a box of 10 Mpc comoving on each size, uniformly resolved with 512^3 particles with mass of $2.95 \times 10^5 M_{\odot}$ each (i.e. ≈ 340 particles for a $10^8 M_{\odot}$ halo). We created initial conditions using our own code *Lizard* (Creasey et al., in prep.) with the Planck cosmology with present day mass fraction $\Omega_M = 0.315$, dark energy $\Omega_{\Lambda} = 0.685$, Hubble constant $H_0 = 67.3 \text{ km s}^{-1} \text{ Mpc}^{-1}$, normalisation $\sigma_8 = 0.829$ and spectral index $n_s = 0.9603$, realised at a redshift of 127.

The gravitational collapse of this dark matter distribu-

tion was evaluated with the N-body code AREPO (Springel 2010), using a softening length of 490 pc physical or 1.95 kpc comoving, whichever is the smaller, and collapsed structures of more than 32 particles identified with SUBFIND.

2.1 Tagging of GCs

In order to infer the orbits of a mass component that has formed in the centres of these early-collapsed halos we tag the most bound particle for all groups with virial mass $M_{200}^{\text{tag}} \geq 10^8 M_{\odot}$ at a redshift of $z_{\text{tag}} = 8.65$, the mass cut chosen to match the number density expected for the MW (later we consider higher and lower mass cuts to examine the effect of this choice). The redshift for tagging in our fiducial model should be interpreted as the average redshift of reionization (a later assembly being assumed unable to form a GC) and has been chosen to be consistent with Planck optical depth constraints (Planck Collaboration et al. 2016). We follow these to redshift zero where the majority of these particles can still be associated with bound structures, however we do not discard those that do not since even if one does not resolve the structure, it is still expected to exist (van den Bosch et al. 2018) and the most bound particle is used as our best tracer for dynamical purposes.

The absent baryonic component of these simulations would (if present) collapse into tightly bound objects (galaxies) with scale lengths of $O(1)$ kpc (e.g. Shen et al. 2003) at the centres of these halos. These will affect the GC population both due to baryonic contraction of the orbits and tidal disruption of those GCs for whom the pericentric distances become comparable to the galactic scale length. The quantification of this we defer until Section 4.

For an overview of our cosmological simulation we show in Fig. 1 a projection of the present day DM density, 7 selected MW-mass halos along with initial ($z = 8.65$) and final ($z = 0$) positions of the tagged GCs in red and green respectively. Immediately apparent is both the strong clustering of the initial GC sites (i.e. these are relatively extreme objects at formation) and the corresponding clustering of their final positions near the centres of massive halos today.

3 THE GC POPULATION

In this section we compare the distribution and dynamics of the halos identified in Sec. 2 with the observations of the globular cluster population. We begin in Sec. 3.1 by examining the number density of GCs per host and then in Sec. 3.2 their spatial distribution within their host halos. When possible we compare only to the low metallicity/blue population. We work under the assumption that the metal rich and red population of GCs is formed in-situ out of baryonic processes in the central galaxy and not well modelled by the hypothesis of GCs formed in their own dark matter halos.

3.1 GC abundance

The most basic question to ask of a GC formation model is whether it predicts the right abundance of GCs as a function of their hosts. The tightest correlation is believed to be between total mass in globular clusters vs. halo mass (Spitler &

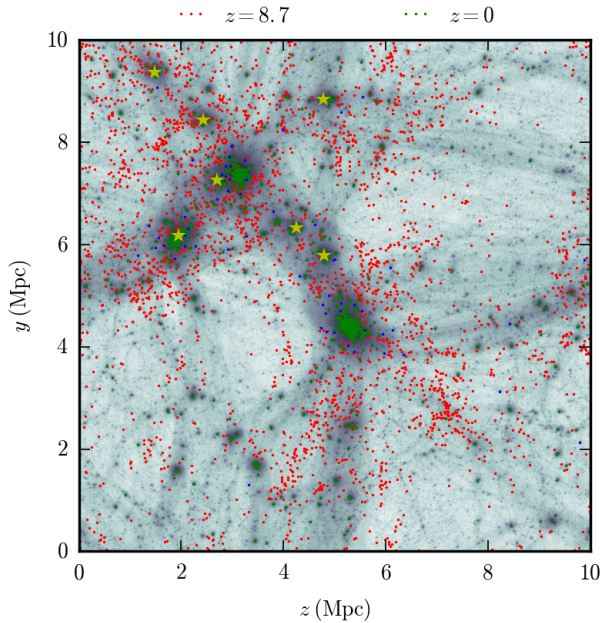


Figure 1. Projection of GC candidate positions identified at redshift 8.7 (*red dots*) as halos of $M_{200} > 10^8 M_{\odot}$ and tracking the most bound particle to redshift 0 (*green dots*), with *blue dots* denoting structures that are still the most massive in their host halos. 7 MW-like halos (see text) have $z=0$ positions denoted by *yellow stars*, and *background shading* represents dark matter density at $z=0$.

Forbes 2009), although one can use GC number as a proxy for GC mass as well (e.g. Blakeslee 1997). Using number of GCs instead of mass eases the comparison with our simulations since we have not followed the detailed baryonic processes (i.e. environment dependent formation and subsequent stripping) which would allow us to assign masses per GC.

As explained in Sec. 2.1, we use our fiducial cut to seed all halos above $M_{\text{vir}} = 10^8 M_{\odot}$ at $z = 8.65$ with a GC. We then follow the most bound particle in these halos at $z = 0$ to predict the position and velocities of those GCs at present day. As shown in Fig. 1, due to hierarchical assembly, painted GCs are today highly clustered around more massive halos, in good agreement with the distribution of observed GCs. We emphasise that this particular choice of tagging parameters is by no means unique; there is a degeneracy between mass and redshift for tagging that can reproduce a similar abundance of subhalos at $z=0$ (see also Diemand et al. 2005). In Fig. 2 we illustrate this degeneracy in terms of the rarity of density peaks given a combination of mass and redshift for tagging. We also include expectations from reionization, in particular, our fiducial tagging corresponds to halos above a reionization temperature of just below 10,000 K at a time consistent with the Planck measurements, although this correspondence is not exact since reionization is expected to be neither instantaneous nor entirely homogeneous. For this reason we consider 5 other combinations of time and mass, indicated with different symbols. A previous estimate by Moore et al. (2006) of the rarity of material needed to forms globular clusters corresponded to halos whose (linear) over-

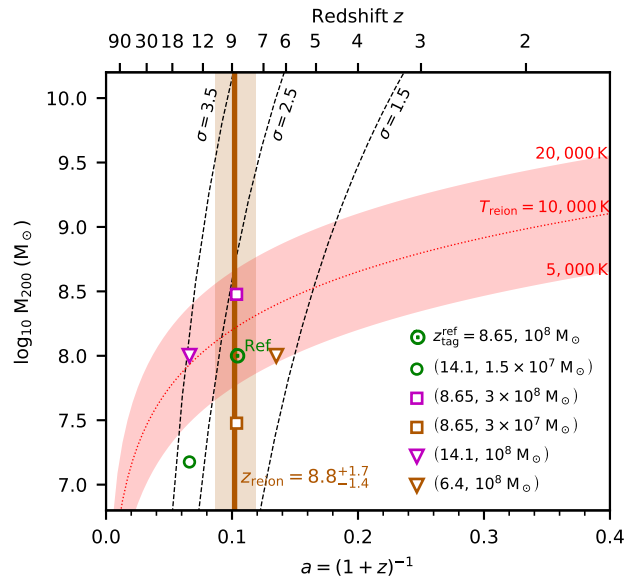


Figure 2. The tagging times (expansion factors) and masses used in this work, in comparison with other constraints. *Dotted green circle* indicates the fiducial $z_{\text{tag}} = 8.65$, $M_{\text{tag}} = 10^8 M_{\odot}$, whilst *open coloured symbols* indicate other taggings (see values inset), with colours corresponding to Fig. 3. *Brown vertical line and shaded* indicate the Planck 2016 reionization time estimate and uncertainty. The *red line* indicates halo masses that correspond to a reionization temperature of 10^4 K, with the effect of raising or lowering to 20,000 K or 5,000 K given by the *red shaded region*. *Labelled black lines* indicate the rarity of these halos (the number of sigma of the expected linear overdensity from the mean, see text). The models in *green* approximately match the number of blue GCs for a $10^{12} M_{\odot}$ halo (see Fig. 3).

densities are approximately 2.5σ above the mean. For comparison we have included the halo mass corresponding to 1.5, 2.5 and 3.5σ (using a sharp- k filter) as a function of expansion factor.

In Fig. 3, we convert these taggings into the number of GCs within the virial radius (defined here as the radius that encloses $200\times$ the critical density) of all identified halos in our simulation output at $z=0$ and plot the resulting abundance of GCs per halo, where we have only included halos with at least 1 GC. This is shown as green solid symbols, using individual dots for halos with more than 8 GCs and otherwise indicating the range with error bars for the 15 and 85th percentiles in mass. This is compared to GC observations in the local group compiled in Mackey (2015), where we have converted V-band magnitude to stellar masses for each host galaxy assuming a mass-to-light ratio of 1 and estimated halo masses based on the abundance matching prescription from Moster et al. (2013). Additionally, local group values (all except for the Milky Way) have been corrected by the estimated fraction of blue GCs using:

$$f_{\text{blue}} = \min\left(\frac{M_{200}}{10^7 M_{\odot}}, 1\right)^{-0.07} \quad (1)$$

taken from Harris et al. (2015). For the MW, we have applied instead a metallicity cut, including all GCs with $\text{Fe}/\text{H} < -1$ as blue (Harris 1996, 2010 edition).

The left panel of Fig. 3 show a reasonable good agree-

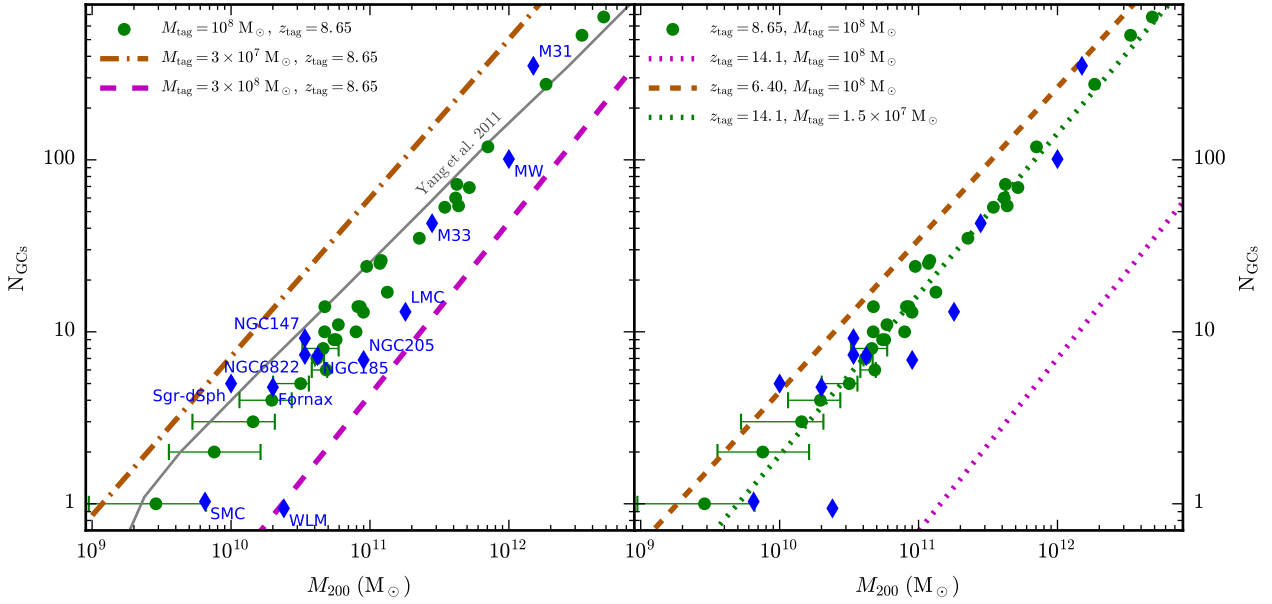


Figure 3. GC counts as a function of halo mass for our simulation (systems with more than 8 GCs are shown as individual *green points*, otherwise we indicate the range with error bars for the 15 and 85th percentiles in mass). *Blue diamonds* indicate the number of inferred blue GCs of local group galaxies (with halo masses inferred from the abundance matching of [Moster et al. 2013](#)) and the fraction of blue GCs using the conversion in Eqn. (1) for all except the MW (where the discrimination is made with Fe/H). *Left panel* shows the expected substructure scaling (from [Yang et al. 2011](#)) in *grey line*. *Coloured dashed lines* indicate the relations for our simulation with different tagging masses, *dashed magenta line* is for $3 \times 10^8 M_{\odot}$ and *dot dashed brown line* is for $3 \times 10^7 M_{\odot}$. In the *right panel* we show the effect of different redshift cuts, with $z_{tag} = 14.1$ in *magenta dotted* and $z_{tag} = 6.4$ in *brown dashed line*. *Green dotted line* shows a combination of a lower mass cut of $M_{tag} = 1.5 \times 10^7 M_{\odot}$ at the higher tagging redshift ($z_{tag} = 14.1$) that has been chosen to match the current blue GC abundances.

ment between local observations and the predictions of our model. We highlight that while the agreement on the *normalisation* is obtained by construction—our fiducial mass cut $10^8 M_{\odot}$ was chosen to reproduce approximately the abundance of blue GCs in the MW, see Sec. 2.1 – the *scaling*, which is almost linear in halo mass, emerges naturally within Λ CDM since the number of high redshift progenitors scales approximately linearly with the halo mass. The grey solid line on the left panel of Fig. 3 corresponds to the scaling of the number subhalos of $10^8 M_{\odot}$ accreted by halos as a function of mass (taken from [Yang et al. 2011](#)). Further discussion of the application of this approach to GCs can be found in [Boylan-Kolchin \(2017\)](#) and [El-Badry et al. \(2018\)](#). One statistic not shown in this plot is the fraction of halos which have no GCs. For our fiducial mass cut, around 50% of galaxies in an $M_{200} \approx 5 \times 10^9 M_{\odot}$ halo (with stellar mass $M_{\star} \approx 10^6 M_{\odot}$) have no GCs, falling sharply with increasing halo mass.

Fig. 3 also explores the effects of assuming a different mass cut (left panel) or redshift cut (right panel) for the tagging of GCs. In agreement with previous work (e.g. [Diemand et al. 2005](#)), more restrictive cuts in terms of density fluctuations at high redshift would result in a lower number of primordial GCs identified around more massive halos today. For example, a higher mass cut $M_{vir} > 3 \times 10^8 M_{\odot}$ to seed GCs (magenta dashed, left panel) or an earlier reionization time $z_{tag} = 14.1$ (magenta dotted line, right panel) is reflected on a smaller fraction of halos qualifying as GCs formation sites and therefore a smaller abundance of GCs per halo at $z = 0$ compared to our fiducial model. On the other

hand, tagging less massive halos (brown dot-dashed line, left panel) or our fiducial mass cut but at a later reionization time $z_{tag} = 6.4$ (brown dashed line, right panel) would both result on a higher GC occupation per halo today. As shown in the next section, these variations on the abundance of GCs given how “rare” the GC-hosting density peaks are at high redshifts correlate strongly with their expected clustering at $z = 0$, which can be used in combination with observations to better constrain this scenario.

3.2 GC spatial distribution

Our next comparison is the predicted radial distribution of GCs around massive hosts at the present day. For reference, the number density of globular clusters in the Galactic halo is observed to decline steeply with distance to the MW, with $n(r) \propto r^{-3.5}$ as average best fit relation (e.g. [Harris 1976](#); [Helmi 2008](#)). This is comparable to the radial distribution of halo stars in numerical simulations of galaxies but is significantly more concentrated than the expected distribution of dark matter or even dwarf satellite galaxies (e.g. [Abadi et al. 2006](#)). We have selected the seven halos in the ‘MW-like’ halo mass range of $M_{200} = 10^{12 \pm 0.5} M_{\odot}$ and checked that the radial distribution obtained is consistent with this value, a fact that has previously been highlighted ([Diemand et al. 2005](#)) as an appealing feature of this mechanism for GC creation (and similarly for halo stars).

However, the galactic GC distribution seems to flatten for the interior 50% of GCs and possibly steepens for the outermost (see e.g. Fig. 7 of [Harris 1976](#)) making the ra-

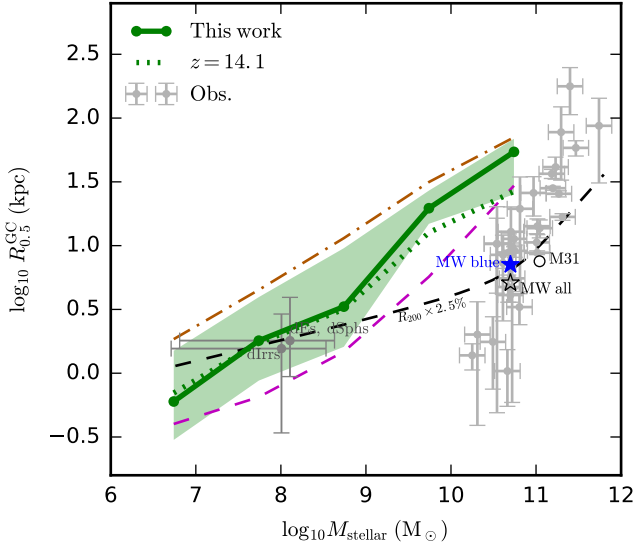


Figure 4. Median radii of GCs from their hosts. *Green line* shows the median relation for our simulation, with *shading* for 15 and 85th percentiles. *Open black star* and *circle* are for the MW and M31 respectively, *filled blue star* is the blue-only GC population for the MW. Observed radii are *grey points* taken from [Hudson & Robison \(2017\)](#) in addition to dLrrs (*orange outline*) and dEs and dSphs (*red outline*) from [Georgiev et al. \(2009\)](#). The black star is the 17 kpc median radius quoted in [Diemand et al. \(2005\)](#). The effect on populations of higher and lower mass cuts (as for Fig. 3) is shown in *magenta dashed* and *brown dot-dashed lines* respectively, and the *green dotted line* represents the $z = 14.1$ cut. *Dashed black line* indicates 2.5% of the virial radius, approximately matching the MW median GC radius.

dial profile of GCs somewhat radius dependent and also well constrained only for the MW and a short handful of other galaxies. An alternative metric to quantify the radial distribution of GCs about their hosts is to use the median distance, i.e. the radius enclosing half the number of GCs per host, which has been recently observationally constrained on hundreds of galaxies over a wide mass range ([Georgiev et al. 2009; Hudson & Robison 2017](#)). In Fig. 4 we show the median half-number size, $R_{0.5}^{\text{GC}}$, predicted by our fiducial model as a function of the stellar mass of the host galaxy at $z = 0$ (green solid line, stellar mass computed assuming abundance matching model by [Moster et al. 2013](#)). Green shaded region indicates the 15%-85% quartiles of the distribution. For our fiducial model, the half number radius of the GC system is comparable to $\sim 14\%$ of the virial radius of the host halos, whilst for the MW it is only about 2.5%, a fraction which we plot for other halo masses for comparison.

The predicted size for the GC distribution can vary with the assumptions made to tag these GCs. For instance, Fig. 4 shows the median half-number radius expected if the mass cut for tagging GCs at $z_{\text{tag}} = 8.6$ is changed to a smaller $M_{200} > 3 \times 10^7$ or larger $3 \times 10^8 M_{\odot}$ compared to our fiducial value. As expected, when the tagged halos are more massive, or correspondingly “rarer” density peaks at z_{tag} , the GCs at $z = 0$ are more clustered (dashed magenta line) than in our fiducial model (solid green). On the other hand, a lower mass cut results in a more extended distribution (dot-dashed brown line). Similar behaviour is observed for a higher or

lower redshift cuts at fixed halo mass. These variations are interesting when combined with predictions for the number of GCs expected in each case. As discussed in Fig. 3, the abundance of GCs within halos at $z = 0$ also depends on the assumptions for tagging, with larger abundances associated to less extreme cuts to host a GC in the early Universe (either lower mass or lower redshift). *This highlights a strong prediction of this model: a fundamental relation between the size of the GCs distribution and the abundance of GCs per host halo at present day.*

We compare the GC distribution in our models to observations in Fig. 4, showing with symbols plus error-bars available measurements on the half-number radius of GCs on external galaxies (data taken from [Georgiev et al. 2009; Hudson & Robison 2017](#))². Data for the blue GC population of the MW (blue star) and M31 (open circle) are taken from in the case of the MW and from [Harris 1996](#), (2010 edition) and for M31 from [Galleti et al. \(2004\)](#) complemented with outer halo clusters from the Pan-Andromeda Archaeological Survey ([Huxor et al. 2014](#)). The result of our fiducial model (chosen to roughly reproduce the abundance of GCs today) is consistent with observations of low mass galaxies ($M_{\text{stellar}} 10^8 M_{\odot}$) but seems to overestimate the sizes of the GC distributions for larger masses. For instance, for stellar masses in the range 10^{10} - $10^{11} M_{\odot}$ the half number radius predicted is 54 kpc (25-69 kpc for 15 & 85th percentiles respectively) which should be compared to the average ~ 10 kpc expected for MW-like galaxies. We have checked that including the effects of baryonic contraction in the central potential of these halos or changing the weight of the tagging technique can shrink the expected sizes by around 6 kpc, but is not enough to bring the results into agreement (see Appendix A for details).

Instead, adopting a higher threshold mass for tagging (magenta curve) helps accommodate the half number radius with observations of the MW, at the expense of explaining the number counts (see Fig. 3). Raising the reionization time to $z_{\text{tag}} = 14.1$ and simultaneously reducing to the tagging mass to fit the number counts (see Fig. 3 green dotted line) also improves the radial distribution, although is still in significant tension with the observations. We have calculated models where an infalling distribution is combined with a compact distribution produced in some galactic process, and find that in order to match the median radii at most 60% of the GCs could come from an infalling population.

At the other extreme, if the GC progenitors were tagged randomly with dark matter particles, their median radii would match that of the dark matter (not shown), at around 90 kpc for the MW and much too extended compared to the observations, even though it would be possible to match the abundances (as shown by [El-Badry et al. 2018](#)).

We note that we have ignored the process of tidal disruption of GCs, that may impact around half of the GCs as they orbit the main halo (e.g. [Prieto & Gnedin 2008; Muratov & Gnedin 2010; Choksi et al. 2018](#), though [Carlberg 2018](#)

² [Hudson & Robison \(2017\)](#) reports the R_e of GC systems, where R_e is the half light radius of the best fit de Vaucouleurs profile to the GCs distribution. [Georgiev et al. \(2009\)](#) results are multiplied by a factor $4/\pi$ to convert the median projected radii to 3D

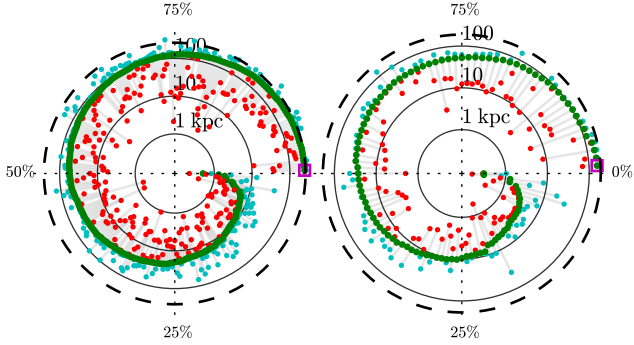


Figure 5. Pericentre, apocentre and current radius for the tagged GCs in the most massive halo (*left panel*) and 2nd-most massive (*right panel*) from Fig. 1. *Red points* indicate the pericentric passage and *cyan points* the apocentre (calculated as in Sec 4). Orbits are ordered in azimuth by their current radius (*green points*, starting from *magenta square*), such that the azimuthal direction is the quantile, with percentiles marked with dotted lines. Labelled *solid lines* indicate radial distances in kpc (spaced logarithmically), whilst the *dashed black line* indicates R_{200} .

have found values nearer unity), where GCs with smaller apocentric radii are preferentially disrupted into streams. Such a preferential removal of GCs would only exacerbate the tension with the observed distribution.

The compact distribution of GCs around the MW has been highlighted before as a hint for an earlier reionization time in our Galaxy ($\tau \sim 15$, see Bekki 2005), which could be a sign of patchy reionization. In fact numerical simulations have shown that larger halos and clusters are believed to reionize earlier due to the UV emission from their progenitors (Alvarez et al. 2009; Li et al. 2014) and partial evidence for this is also found in observations (Spitler et al. 2012). A higher than average redshift of reionization for the MW seems preferred not only from their GC distribution but would also help alleviate the missing satellite problem in the Local Group (Busha et al. 2010; Li et al. 2014). However, we notice that the MW or even M31 in Fig. 4 are not far from the average of external galaxies with the same mass, and therefore GC formation models should be able to account for this rather compact GC distribution without invoking particular outliers in the reionization history. Based on our results, current measurements for half number radius of metal poor GCs suggest that about half and up to 60% of GCs in MW-like objects could have been formed in early-collapsed halos at high redshift. In what follows, we study their expected kinematics.

4 ORBITS AND DYNAMICS OF GCS

GCs that formed at the centres of their own DM halos will follow orbits and kinematics predicted primarily by the Λ CDM scenario. We use our simulations and tagging technique to explore the present-day orbits of GCs around MW-mass hosts. Unless explicitly mentioned, we focus on our fiducial tagging model, although the results presented do not depend significantly on this assumption.

Dark matter halos within Λ CDM have radially biased orbits (Wojtak et al. 2009, 2013) with apocentres that are significantly larger than the pericentres. Numerical simulations have shown that subhalos (and therefore satellite galaxies inhabiting those subhalos) inherit such elliptical orbits (Sales et al. 2007; Iannuzzi & Dolag 2012), an effect that contributes to the disruption and lowering of star formation in satellites, even for those seemingly today in the outskirts of groups and clusters. If blue GCs – or a fraction of them – are expected to form within DM halos, we might expect their orbits to have an ellipticity comparable to satellites, with present-day positions correlating poorly with their minimum distance to their hosts.

In order to characterise the orbits of our GC candidates we need a time sampling that is significantly higher than the outputs of the snapshots in the simulation. A more accurate orbit parameter estimation can be achieved by taking the present day position and velocity of GCs and integrating their orbits in an analytical potential. We approximate the host potentials as NFW profiles (Navarro et al. 1997). The two NFW parameters are the M_{200} and the scale radius r_s (determined from the relation $r_s \approx R_{\text{max}}^{\text{vel}}/2.16$, where $R_{\text{max}}^{\text{vel}}$ is the radius of maximum circular velocity in the spherically averaged mass profile). The pericentric and apocentric orbital passages of the GC candidates are then calculated from the radial and tangential velocity components v_r and v_\perp relative to the halo centres, along with their current radius.

As an example, we show in Fig. 5 the relation between present day distance (green), pericentre (red) and apocentres (cyan) of tagged GCs for the two most massive MW-like halos in our simulation. In this polar representation, GCs are sorted according to their present day distance, moving counter-clockwise from the furthest to the nearest and starting on the right magenta square. Solid thin lines indicate lines of constant radius at 1, 10 and 100 kpc from the host, while the dashed circle indicates the virial radius of the system 260 and 189 kpc for left and right, respectively). A circular orbit in this representation would have three distances coinciding on the same point. Instead, an elliptical orbit has a large separation between the corresponding red and cyan dots, with the green symbol at some intermediate distance according to the phase of the orbit.

Fig. 5 highlights that, as expected, GCs formed with this cosmological origin are characterised by quite elliptical orbits, with apocentres that are on average (median) a factor ~ 4 farther than their pericentres. However variations can be large, with a significant fraction of GCs that today are found near ~ 100 kpc that could have ventured in the past within just 10 kpc of their hosts. Interestingly, this figure also highlights an important prediction: very few (although non zero) number of GCs have apocentric distances that go beyond the R_{200} of the system and may be interpreted in observations as “intra-galactic” objects when they are actually bound. We return to quantifying this in Sec. 5.

The large ellipticity in GCs orbits means that they could have been in the past exposed to much stronger tidal forces than estimated for their present day position, with important consequences on the GCs tidal disruption and, especially, of their surrounding dark matter subhalo. Indeed, Fig. 5 suggests that the dark matter content of GCs shall not be judged as intact even for GCs that *today* are seen in

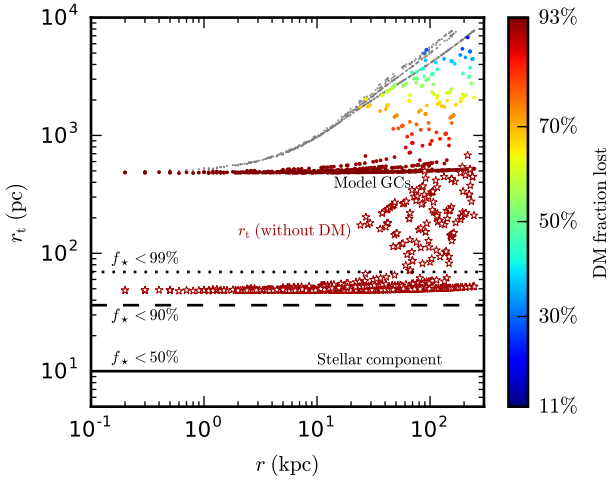


Figure 6. Estimate of the tidal truncation radius from their pericentric passages, with and without the DM halo, for the GCs around the 7 model MWs from Fig. 1. *Coloured points* indicate the tidal radius using the DM satellite mass in Eqn. (2), where the colours correspond to the fraction of DM stripped (from 11-93%). *Red stars* indicate the tidal radius using only the stellar component (i.e. for those where the DM halo has been stripped). For comparison, *horizontal black solid, dashed and dotted lines* indicate a fiducial GC stellar distribution, as the radii that contain 50, 90 and 99% of the stellar fraction.

the outskirts of their hosts. How much of their initial dark matter mass might still be associated to blue GCs is therefore dependent not only on their current distance but also of their past orbital history. For instance, at our resolution, only 20% of the GC-hosting subhalos whose most bound particle is around 100 kpc today has retained a resolved DM-substructure that is identified by our subhalo finder (32 particles or more). This number, although indicative of the overall trend, is certainly strongly dependent on the numerical resolution of our simulation (see e.g. [van den Bosch et al. 2018](#)). Instead, we estimate analytically the expected truncation radius and retained dark matter mass fraction for the subhalos in Fig. 6.

To be conservative, we estimate the tidal radius and retained mass fraction at the pericentric distance, when the background potential is maximal and the effects of tidal disruption are strongest. Taking the best-fit NFW profile to our MW-like host halos, we estimate the tidal radius r_t of our tagged subhalos from

$$\left(\frac{r_t}{r}\right)^3 = \frac{M_{\text{sat}}}{\left(2 - \frac{d \ln M_{\text{host}}}{d \ln r}\right) M_{\text{host}}(< r)} \quad (2)$$

with M_{host} and M_{sat} the total mass of the host and satellite dark matter halo (see [Springel et al. 2008](#)), and r being either the pericentric distance to the host or the current distance (see Fig. 6). We also account for the effects of baryons in the central halo by adding to the potential a disk of mass $10^{11} M_{\odot}$ and scale radius 3 kpc. As shown in Fig. 6, the tidal field of the MW generally only strips the subhalos down to > 500 pc, well above the observed half-light radius of the stars in GCs ($r_h \lesssim 10$ pc, see solid black line), even for orbits with small pericentric passages. This is somewhat misleading, however, since many of these will have lost the

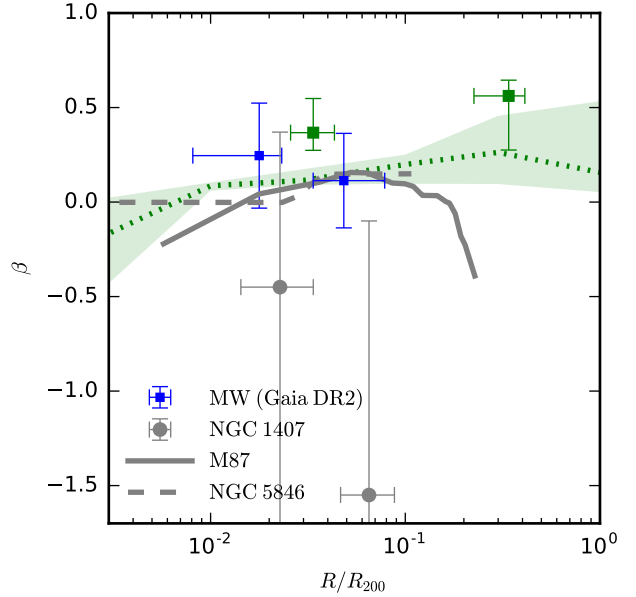


Figure 7. Velocity anisotropy (β) as a function of distance normalised to the virial radius for the GCs in the 7 MW mass halos from our simulations (*green square symbols*). Due to low number statistics we show only 2 radial bins. Error-bars correspond to the 15-85% percentiles. GCs in this scenario are expected to be on strongly biased radial orbits ($\beta \geq 0.3$) which are slightly more radial than the underlying dark matter particles in the host halo (*green dotted line and shaded region* showing the 15-85th percentiles of the distribution). We compare with a few available observations from the literature: GC anisotropies for the blue GCs of the MW are shown in *blue squares* with errors, for M87 are shown as the *solid grey line* (from [Zhu et al. 2014](#), Fig. 12), for NGC 5846 in *dashed grey* (from [Napolitano et al. 2014](#), Fig. 5), and for NGC 1407 in *grey circles with error bars* (from [Spitler et al. 2012](#), Fig. 3).

majority of the dark matter (these tidal radii correspond to 11-93% of their dark matter). If the DM stripping becomes non-linear (e.g. for multiple pericentric passages), then the relevant satellite mass in Eqn. (2) is only the stellar mass, and we additionally plot the calculation for these in Fig. 6 (star symbols). For comparison we also show enclosed mass fractions for a fiducial [King \(1966\)](#) profile with half mass radius of 10 pc and concentration 1.5, and the overlap of a significant fraction suggests that many of these would have appreciable tidal tail, such as those seen in [Carlberg \(2017\)](#).

Whether or not the DM content of the relatively undisturbed subhalos should still be observable is the subject of study of a forthcoming paper (Creasey et al., *in prep*), but we highlight here that one of the strongest predictions of this GC formation model, namely the existence of a massive and extended dark matter halo surrounding each GC, should be evaluated with care due to the highly radial orbital structure expected in this scenario for GCs around their host galaxies added to the very compact distribution of stars mapping too little of the expected extension of this dark matter component.

An alternative way to quantify the ellipticity of the or-

bits is through the anisotropy parameter β defined as:

$$\beta = 1 - \frac{1}{2} \frac{\langle v_{\perp}^2 \rangle}{\langle v_{\parallel}^2 \rangle}, \quad (3)$$

where $\langle v_{\perp}^2 \rangle$ and $\langle v_{\parallel}^2 \rangle$ are the velocity dispersion in the radial and tangential directions. Even in a simulation where there is no uncertainties on the tracer velocities this generally requires large sample sizes (since both quantities need to be estimated), and so we compute the average β profile of the tagged GCs as a function of distance (normalised to the virial radius) for the stacked sample of our 7 MW-mass halos in two radial bins (median and 15-85% percentiles shown in green square symbols with error-bars), which we choose located at 0.03 and 0.3 R_{200} . As expected from Fig. 5 the predicted orbital structure for GCs is strongly biased radially ($\beta > 0$), in particular at large radii. Notice that the anisotropy of the orbits of GCs traces roughly that one of the underlying dark matter halo of the host (see green dotted and shaded regions), although with slightly larger radial component than the dark matter particles (in agreement with Diemand et al. 2005).

Observationally, measuring the anisotropy of GCs is an even more challenging task, however some observational constraints are becoming available. For the case of the MW, Gaia Collaboration et al. (2018) provide proper motions for 75 GCs, and we show the velocity anisotropy estimated for the blue GCs in two radial bins in Fig. 7. Although not strongly constraining (primarily due to the low number statistics), they do suggest a small positive radial anisotropy consistent with a radial infall model.

Beyond the MW, for other external $\sim L_*$ galaxies (e.g. M31) one can apply spherical Jeans modelling to infer the missing components³, but the mass-anisotropy degeneracy introduces a large additional uncertainty (e.g. Diakogiannis et al. 2014) that limits the utility of the β measurements at present. Instead, the situation is more promising for GCs in cluster sized halos (which have correspondingly many more GCs) and Zhu et al. (2014); Napolitano et al. (2014) and Spitler et al. (2012) have inferred anisotropy profiles from these for M87, NGC 5846 and NGC 1407 respectively, with $M_{200} \approx 10^{13} - 10^{15} M_{\odot}$, which we show in grey curves and symbols for comparison in Fig. 7. Note that for the Virgo cluster there is some additional uncertainty in that the cluster may not be relaxed (Binggeli et al. 1987; Strader et al. 2011).

Taken at face value, Fig. 7 suggests that GCs formed cosmologically in their own dark matter halos prior to infall into their (larger) present day hosts would have a larger radial velocity anisotropy than is observed for real systems. However we caution that one cannot make strong conclusions due to the size of the uncertainty in observations and the fact that our predictions are for MW-mass systems and observational constraints are only available for larger group and cluster halos.

³ In the case of M31 the GC spatial and velocity correlations are visually apparent (Djorgovski et al. 1997), previously Veljanoski et al. (2014) assumed an isotropic ($\beta = 0$) velocity dispersion in the 30-100 kpc range.

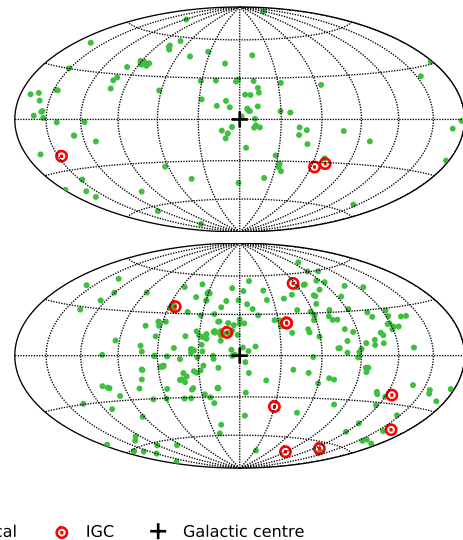


Figure 8. Sky distribution of simulated “intergalactic” GCs (red dotted circles), defined as those laying within $[1-3] R_{200}$ of a MW-like halo and not bound to any other system with $M_{200} > 3 \times 10^8 M_{\odot}$ (i.e. not belonging to any other halo of a field dwarf). We plot the GC distribution from an Earth-like vantage: 8 kpc from the centres of the two most massive MW-like halos (halos as for Fig. 5). *Green dots* denote (local) “normal” candidates within R_{200} and *red dotted circles* denote the isolated GC candidates. *Black plus* indicates the direction to the halo centre. This scenario predicts very few intergalactic GCs, with bounds consistent with the current lack of observational candidates (see text for more detail).

Regardless, it seems interesting that at large radii several observations suggest tangential velocity anisotropy (i.e. $\beta < 0$), which seems difficult to accommodate in this scenario. In fact, radial anisotropies (especially at large radii) are not limited to this model only. For instance one would also expect this if GCs were formed either in the main galaxy and ejected (since GCs with a distant orbital apocentre would still be expected to have a near pericentre and thus a nearly radial orbit) and similarly if outer GCs were stripped from satellites (which would also need to be on quite radial orbits to be significantly affected by tidal disruption during close pericentre passages). Mechanisms such as preferential destruction of GCs on radial orbits can be invoked, but as we saw earlier this is expected to affect only a modest fraction, and as such observations suggesting tangential anisotropies beyond 20% of R_{200} remain a puzzle. This unusual dynamical arrangement of GCs seems reminiscent of the ‘planes of (accreted) satellites’ of M31 (Koch & Grebel 2006) - an arrangement that in Λ CDM is unlikely although not exceptional (Cautun et al. 2015).

5 THE ABUNDANCE OF INTERGALACTIC GLOBULAR CLUSTERS

One attractive avenue for the discrimination of GC formation models is the presence or absence of isolated/free GCs at the present day floating outside more massive hosts. Since

the model where one populate the high-sigma peaks at high redshift causes GC progenitors to lie *outside* galaxies at their formation, some fraction of these could still be isolated from galaxies today (so-called Intergalactic Globular Clusters or IGCs) inhabiting their own dark matter halo. This is in contrast with models where GCs are the result of baryonic formation processes in galaxies and essentially remain associated to the galactic halos for their entire lifetimes (excluding some almost vanishingly small fraction that are ejected during halo interactions and whose resulting orbit fails to be incorporated in either halo). It is important to keep in mind, however, that the high-sigma peaks at high z are still strongly clustered, and the vast majority will be incorporated into larger halos at redshift zero as a result of this (see for instance Fig. 1)

On the observational side the result is a null one, i.e. there are no observed isolated (i.e. not bound to the halo of a galaxy) GCs. Marginal cases exist, for example Crater/Laevens I (Belokurov et al. 2014; Laevens et al. 2014) at ≈ 150 kpc, however this still puts it inside R_{200} for the MW (≈ 240 kpc, e.g. Springel et al. 2008). Nevertheless the observational volume over which we can be confident of completeness is limited. di Tullio Zinn & Zinn (2015) searched the Sloan Digital Sky Survey (SDSS) and none of the GCs they found appear to be truly isolated (Mackey et al. 2016), which from their figures is complete to a depth of around 750 kpc (around the distance of M31, and smaller than the ≈ 1 Mpc extent of the Local Group) and the SDSS footprint is around $14,555^\circ$ (around 30% of the sky) which gives a volume of around 0.5 Mpc^3 .

To evaluate the level of this constraint quantitatively means we would like to know the abundances of these IGCs inferred from our N-body simulation. Notably in Λ CDM the regions from $1-3R_{200}$ will on average be several tens of times denser than the mean density of the Universe (even excluding that the Local Group is a loose ‘group’ containing M31, suggesting a density higher than average for a MW mass galaxy, discussed further in Creasey et al. 2015) and correspondingly one could expect the density of GCs to be much higher too. In order to evaluate this we took the 7 MW-mass halos in our simulated box and counted GCs that are both in the range $1-3R_{200}$ and *not* incorporated into any other halo above $3 \times 10^8 M_\odot$ ($3 \times$ the mass threshold, and thus significant halo growth usually associated with the merger into a LG galaxy). A sky-projection for such intergalactic GCs is shown for our two most massive halos in Fig. 8 (see red dotted symbols). These maps assume solar-like position 8 kpc from the centre of the halo and we have marked for completeness “normal” GCs that are within R_{200} (green dots). Isolated GCs show, as expected, little clustering.

We find that isolated GCs are indeed very rare, with the most massive halo having only 9 in this range (lower panel) and the second most massive only 3 (upper panel). Combining all our data together gives an abundance measure for GCs between 1 and $3R_{200}$, denoted N_{13} , of

$$N_{13} = 4.7 \times \left(\frac{M_{200}}{10^{12} M_\odot} \right), \quad (4)$$

where we have assumed a linear scaling with halo mass and had to apply a volume correction of a couple of percent due to a slight overlap of the $R = 3R_{200}$ spheres of the seven halos. For comparison we have repeated this calculation for

the higher redshift tagging ($z = 14.1$, $M_{\text{tag}} = 1.5 \times 10^7 M_\odot$) and found this reduces the prefactor by around 40% to 2.77, i.e. as one might expect from their higher clustering at high redshift that they are less common in the field today. The value of 4.7 for a fiducial $10^{12} M_\odot$ MW halo would correspondingly suggest that for 30% of the sky (i.e. the SDSS result from di Tullio Zinn & Zinn 2015 and Mackey et al. 2016) the expected value would be 1.4 IGCs and, assuming Poisson statistics, that the probability of observing zero is $\exp(-1.4) \approx 25\%$, and easy to accommodate (by extension also true for the higher redshift cut). In the future, as more GCs are identified in the outskirts of our galaxy, the observation of isolated GCs free floating between galaxies might become an exciting constraint to the models.

6 SUMMARY AND CONCLUSIONS

Old globular clusters have ages comparable to the Hubble time, the remaining uncertainty around which has significant implications for their formation. A late formation hypothesis ($z \approx 4$) would indicate a galactic origin (either in the MW or its progenitors and satellites) whilst an early formation ($z \approx 10$) would be compatible with them forming at the centres of their own dark matter halos in the most massive halos at that time (a.k.a high density sigma peaks, Diemand et al. 2005).

In this work we study various implications of the latter hypothesis and examine their constraining power when compared to local available observations. We perform an N-body cosmological simulation of a 10 Mpc box where we are able to resolve halos with $M_{200} > 10^7 M_\odot$. We employ a tagging technique to identify the GC-forming halos at high redshift and trace their positions to the present day. In agreement with previous studies, we find that choosing rare sigma peaks (massive halos) at high redshift as formation sites for metal poor GCs lead to a highly clustered distribution of GCs today around more massive galaxies, a simple consequence of the hierarchical nature of Λ CDM.

Interestingly, we find that such simple assumption and tagging process automatically generates a GC abundance per halo that is almost linear in halo mass, in good agreement with the observed relation between the number or mass of GCs and host halo mass (Hudson et al. 2014). The normalisation of that scaling depends sensitively on the mass of the GC bearing halos and the redshift of tagging. Once both are fixed, this has consequences for both, the abundance and the radial distribution of GCs at present day. We find that using both properties combined can place strong constraints on this formation scenario for GCs. Namely, early redshifts and higher masses assumed for tagging result on more centrally concentrated radial distributions and correspondingly also a lower number of GCs per host.

If one chooses a mass and redshift cut consistent with the observed abundance of GCs (in our model this occurs for $M_{200} = 10^8 M_\odot$ and $z_{\text{tag}} = 8.65$, adopted as our fiducial model), the obtained radial distribution is too extended around MW-like hosts compared to observations. For example, the observed radius containing half of the MW blue GCs population is 7.1 kpc, compared to ~ 54 kpc median in our fiducial model. Fitting the observed half number radius of GCs would require us to assume a more strongly biased

population of halos forming GCs at high redshift, which results on a lower $z = 0$ abundance that can account for only 50-60% the observed number of metal poor GCs in MW-like systems.

We conclude that although this formation scenario might not explain *all* the observed blue GCs in MW-like halos, it can account for about 50-60% of it according to the current observational constraints. Notice that some of this tension would be alleviated if the MW and other nearby galaxies were somehow special, which might be the case if reionization was inhomogeneous (Spitler et al. 2012). However, as the radial distribution of GCs around other MW-mass galaxies have become available, it appears more unlikely that the MW is an outlier and consequently may need a different explanation for their rather compact distribution of metal poor GCs. Encouragingly, this formation scenario seems to predict the correct abundance and radial extension of metal poor GCs in dwarf galaxies.

As such, it is worth exploring further the other predictions of this formation model in terms of kinematics and distribution of GCs. Peak-models naturally set up a radial velocity anisotropy where GCs navigate into the galactic halo on preferentially relatively radial orbits ($\beta > 0.3$). Counter-intuitively there are a number of observations that suggest either isotropic or even tangential velocity anisotropies from tracer material in the halos, albeit the best evidence comes from larger halos (clusters) and require strong assumptions of equilibrium and mass distribution. Our N-body simulations suggest that the intrinsic scatter in the outer halo (which is primarily caused by substructure) can be quite large, meaning that the constraining power based on a handful of either observed or simulated objects is rather weak. Cluster scale larger volume simulations would be required on the theoretical side.

The high ellipticity expected for GC orbits also means that a large fraction of GCs must have passed within only a few dozen kpc of the centre of the host, even for those GCs currently populating the outskirts of halos. Analytical estimates based on the orbits in our simulations indicate that the majority of GCs have lost at least half of their initially bound dark matter mass, and even GCs today at distances as far as 100 kpc can be heavily stripped, retaining only 30% of dark matter on average but down to 7% for those in the most highly radial orbits. This should be kept in mind when attempting dynamical modelling of the stars in GCs (e.g. Conroy et al. 2011). We will address the consequences for the dark matter content of GCs formed in this scenario in more detail in a forthcoming paper (Creasey et al., *in prep*).

One strong constrain to this model is the fact that despite significant observational efforts, no detection of truly isolated GCs (i.e. those not associated with the halo of any galaxy) has been made so far (e.g. di Tullio Zinn & Zinn 2015; Mackey et al. 2016). Our model predicts that intergalactic GCs should be, indeed, extremely rare and considerations of the volume explored in observations retrieves a predicted detection of ≈ 1.4 GC, consistent within Poisson noise with the current null detection in observational campaigns.

Our results support a scenario where more than half of the blue GCs could have formed within their own dark matter halos at high redshift before reionization. Due to the hierarchical and self-similar nature of substructure within

Λ CDM this simple model provides strong predictions for the abundance, radial distribution and kinematics of such population.

Although the detection of a large dark matter component surrounding some of these GCs is the most tempting evidence for this formation scenario, the devil could instead be in the details; and a more systematic joint study of number, radial distribution and kinematics of observed GCs around other large systems might prove equally fruitful at constraining GC formation scenarios. In the MW itself, the detection of a GC candidate associated to the ultra-faint dwarf Eri II prompts the idea of at least some GCs being hosted by undetected surrounding dark matter halos (Zaritsky et al. 2016). As the cosmological place of GCs continues to be studied, it must not be discarded that the oldest and more metal poor GCs could have originated in the hearts of early collapsed dark matter halos, constituting the easiest to observe and therefore most accessible reionization fossils available to our telescopes today.

ACKNOWLEDGEMENTS

The authors would like to thank Marcelo Alvarez, Oleg Gnedin, Raul Angulo and Alessia Longobardi for useful discussions, Volker Springel for making AREPO available for this work. We would also like to thank the anonymous referee for comments which significantly improved this work. We are grateful to the hospitality of the Kavli Institute for Theoretical Physics (KITP) at which some of this work was written, under a research programme supported in part by the National Science Foundation under Grant No. NSF PHY11-25915. LVS acknowledges support from the Hellman Foundation and HST grant HST-AR-14583. OS acknowledges support by NASA MUREP Institutional Research Opportunity (MIRO) grant number NNX15AP99A.

REFERENCES

- Abadi M. G., Navarro J. F., Steinmetz M., 2006, *MNRAS*, **365**, 747
- Adamo A., Kruijssen J. M. D., Bastian N., Silva-Villa E., Ryon J., 2015, *MNRAS*, **452**, 246
- Alvarez M. A., Busha M., Abel T., Wechsler R. H., 2009, *ApJ*, **703**, L167
- Aubert D., et al., 2018, *ApJ*, **856**, L22
- Bastian N., Cabrera-Ziri I., Davies B., Larsen S. S., 2013, *MNRAS*, **436**, 2852
- Bekki K., 2005, *ApJ*, **626**, L93
- Belokurov V., Irwin M. J., Koposov S. E., Evans N. W., Gonzalez-Solares E., Metcalfe N., Shanks T., 2014, *MNRAS*, **441**, 2124
- Binggeli B., Tammann G. A., Sandage A., 1987, *AJ*, **94**, 251
- Blakeslee J. P., 1997, *ApJ*, **481**, L59
- Blumenthal G. R., Faber S. M., Flores R., Primack J. R., 1986, *ApJ*, **301**, 27
- Bovill M. S., Puzia T. H., Ricotti M., Taylor M. A., 2016, *ApJ*, **832**, 88
- Boylan-Kolchin M., 2017, preprint, ([arXiv:1705.01548](https://arxiv.org/abs/1705.01548))
- Busha M. T., Alvarez M. A., Wechsler R. H., Abel T., Strigari L. E., 2010, *ApJ*, **710**, 408
- Carlberg R. G., 2017, *ApJ*, **838**, 39
- Carlberg R. G., 2018, *ApJ*, **861**, 69
- Cautun M., Bose S., Frenk C. S., Guo Q., Han J., Hellwing W. A., Sawala T., Wang W., 2015, *MNRAS*, **452**, 3838

- Choksi N., Gnedin O. Y., Li H., 2018, *MNRAS*, **480**, 2343
- Cohen J. G., 2004, *AJ*, **127**, 1545
- Conroy C., Loeb A., Spergel D. N., 2011, *ApJ*, **741**, 72
- Creasey P., Scannapieco C., Nuza S. E., Yepes G., Gottlöber S., Steinmetz M., 2015, *ApJ*, **800**, L4
- Deason A. J., Van der Marel R. P., Guhathakurta P., Sohn S. T., Brown T. M., 2013, *ApJ*, **766**, 24
- Diakogiannis F. I., Lewis G. F., Ibata R. A., 2014, *MNRAS*, **443**, 598
- Diemand J., Madau P., Moore B., 2005, *MNRAS*, **364**, 367
- Djorgovski S. G., Gal R. R., McCarthy J. K., Cohen J. G., de Carvalho R. R., Meylan G., Bendinelli O., Parmeggiani G., 1997, *ApJ*, **474**, L19
- Dutton A. A., van den Bosch F. C., Dekel A., Courteau S., 2007, *ApJ*, **654**, 27
- El-Badry K., Quataert E., Weisz D. R., Choksi N., Boylan-Kolchin M., 2018, preprint, ([arXiv:1805.03652](https://arxiv.org/abs/1805.03652))
- Forbes D. A., 2017, *MNRAS*, **472**, L104
- Gaia Collaboration et al., 2018, preprint, ([arXiv:1804.09381](https://arxiv.org/abs/1804.09381))
- Galletti S., Federici L., Bellazzini M., Fusi Pecci F., Macrina S., 2004, *A&A*, **416**, 917
- Georgiev I. Y., Hilker M., Puzia T. H., Goudfrooij P., Baumgardt H., 2009, *MNRAS*, **396**, 1075
- Georgiev I. Y., Puzia T. H., Goudfrooij P., Hilker M., 2010, *MNRAS*, **406**, 1967
- Goddard Q. E., Bastian N., Kennicutt R. C., 2010, *MNRAS*, **405**, 857
- Griffen B. F., Drinkwater M. J., Thomas P. A., Helly J. C., Pimblet K. A., 2010, *MNRAS*, **405**, 375
- Griffen B. F., Drinkwater M. J., Iliev I. T., Thomas P. A., Mellema G., 2013, *MNRAS*, **431**, 3087
- Harris W. E., 1976, *AJ*, **81**, 1095
- Harris W. E., 1996, *AJ*, **112**, 1487
- Harris W. E., Harris G. L., Hudson M. J., 2015, *ApJ*, **806**, 36
- Helmi A., 2008, *A&ARv*, **15**, 145
- Hudson M. J., Robison B., 2017, preprint, ([arXiv:1707.02609](https://arxiv.org/abs/1707.02609))
- Hudson M. J., Harris G. L., Harris W. E., 2014, *ApJ*, **787**, L5
- Huxor A. P., et al., 2014, *MNRAS*, **442**, 2165
- Iannuzzi F., Dolag K., 2012, *MNRAS*, **427**, 1024
- Ibata R., Nipoti C., Sollima A., Bellazzini M., Chapman S. C., Dalessandro E., 2013, *MNRAS*, **428**, 3648
- Iliev I. T., Moore B., Gottlöber S., Yepes G., Hoffman Y., Mellema G., 2011, *MNRAS*, **413**, 2093
- Kimm T., Cen R., Rosdahl J., Yi S. K., 2016, *ApJ*, **823**, 52
- King I. R., 1966, *AJ*, **71**, 64
- Koch A., Grebel E. K., 2006, *AJ*, **131**, 1405
- Krauss L. M., Chaboyer B., 2003, *Science*, **299**, 65
- Kravtsov A. V., Gnedin O. Y., 2005, *ApJ*, **623**, 650
- Kruijssen J. M. D., 2015, *MNRAS*, **454**, 1658
- Laevens B. P. M., et al., 2014, *ApJ*, **786**, L3
- Lane R. R., et al., 2010, *MNRAS*, **406**, 2732
- Law D. R., Majewski S. R., 2010, *ApJ*, **718**, 1128
- Li T. Y., Alvarez M. A., Wechsler R. H., Abel T., 2014, *ApJ*, **785**, 134
- Li H., Gnedin O. Y., Gnedin N. Y., Meng X., Semenov V. A., Kravtsov A. V., 2017, *ApJ*, **834**, 69
- Lunnan R., Vogelsberger M., Frebel A., Hernquist L., Lidz A., Boylan-Kolchin M., 2012, *ApJ*, **746**, 109
- Mackey D., 2015, *Globular Clusters in the Local Group*. Springer International Publishing, p. 215, doi:10.1007/978-3-319-10614-4_18
- Mackey A. D., Beasley M. A., Leaman R., 2016, *MNRAS*, **460**, L114
- Mistani P. A., et al., 2016, *MNRAS*, **455**, 2323
- Moore B., Diemand J., Madau P., Zemp M., Stadel J., 2006, *MNRAS*, **368**, 563
- Moster B. P., Naab T., White S. D. M., 2013, *MNRAS*, **428**, 3121
- Muratov A. L., Gnedin O. Y., 2010, *ApJ*, **718**, 1266
- Naoz S., Narayan R., 2014, *ApJ*, **791**, L8
- Napolitano N. R., Pota V., Romanowsky A. J., Forbes D. A., Brodie J. P., Foster C., 2014, *MNRAS*, **439**, 659
- Navarro J. F., Frenk C. S., White S. D. M., 1997, *ApJ*, **490**, 493
- Peñarrubia J., Varri A. L., Breen P. G., Ferguson A. M. N., Sánchez-Janssen R., 2017, preprint, ([arXiv:1706.02710](https://arxiv.org/abs/1706.02710))
- Peebles P. J. E., 1984, *ApJ*, **277**, 470
- Peng E. W., et al., 2006, *ApJ*, **639**, 95
- Pfeffer J., Kruijssen J. M. D., Crain R. A., Bastian N., 2018, *MNRAS*, **475**, 4309
- Planck Collaboration et al., 2016, *A&A*, **594**, A13
- Press W. H., Schechter P., 1974, *ApJ*, **187**, 425
- Prieto J. L., Gnedin O. Y., 2008, *ApJ*, **689**, 919
- Renaud F., Agertz O., Gieles M., 2017, *MNRAS*, **465**, 3622
- Ricotti M., Parry O. H., Gnedin N. Y., 2016a, *ApJ*, **831**, 204
- Ricotti M., Parry O. H., Gnedin N. Y., 2016b, *ApJ*, **831**, 204
- Sales L. V., Navarro J. F., Lambas D. G., White S. D. M., Croton D. J., 2007, *MNRAS*, **382**, 1901
- Shen S., Mo H. J., White S. D. M., Blanton M. R., Kauffmann G., Voges W., Brinkmann J., Csabai I., 2003, *MNRAS*, **343**, 978
- Spitler L. R., Forbes D. A., 2009, *MNRAS*, **392**, L1
- Spitler L. R., Romanowsky A. J., Diemand J., Strader J., Forbes D. A., Moore B., Brodie J. P., 2012, *MNRAS*, **423**, 2177
- Springel V., 2010, *MNRAS*, **401**, 791
- Springel V., et al., 2008, *MNRAS*, **391**, 1685
- Strader J., et al., 2011, *ApJS*, **197**, 33
- Taylor M. A., Puzia T. H., Gomez M., Woodley K. A., 2015, *ApJ*, **805**, 65
- Veljanoski J., Helmi A., 2016, *A&A*, **592**, A55
- Veljanoski J., et al., 2014, *MNRAS*, **442**, 2929
- Wojtak R., Lokas E. L., Mamon G. A., Gottlöber S., 2009, *MNRAS*, **399**, 812
- Wojtak R., Gottlöber S., Klypin A., 2013, *MNRAS*, **434**, 1576
- Yang X., Mo H. J., Zhang Y., van den Bosch F. C., 2011, *ApJ*, **741**, 13
- Zaritsky D., Crnojević D., Sand D. J., 2016, *ApJ*, **826**, L9
- Zepf S. E., Ashman K. M., 1993, *MNRAS*, **264**, 611
- Zhu L., et al., 2014, *ApJ*, **792**, 59
- di Tullio Zinn G., Zinn R., 2015, *AJ*, **149**, 139
- van den Bergh S., 2000, *ApJ*, **530**, 777
- van den Bosch F. C., Ogiya G., Hahn O., Burkert A., 2018, *MNRAS*, **474**, 3043

APPENDIX A: TESTS ON GC RADIAL DISTRIBUTIONS

One should consider the baryonic effects that we have ignored in this scenario. Specifically, we have ignored tidal stripping, which will preferentially remove GCs nearest the centre and *increase* our median radii (although this will primarily affect the metal-rich population) and increase the tension. Thus from this perspective, the radius reported here should be considered *lower* limits to the expected half-number radii. On the other hand the baryonic collapse of material to the centres of halos will contract the orbits and tend to alleviate the tension. Using the adiabatic approximation for circular orbits (e.g. Blumenthal et al. 1986) we also indicate the the contracted radii where we assume a $10^{12} M_{\odot}$ halo with a median concentration of 8.6. This gives a contraction of approximately 6 kpc for most of the halos of interest, though this is probably an overestimate due to the circular orbit approximation (e.g. Dutton et al. 2007). For an easy comparison, we have indicated the effect of baryonic contraction in our set of Aquarius halos shown in Fig. 4,

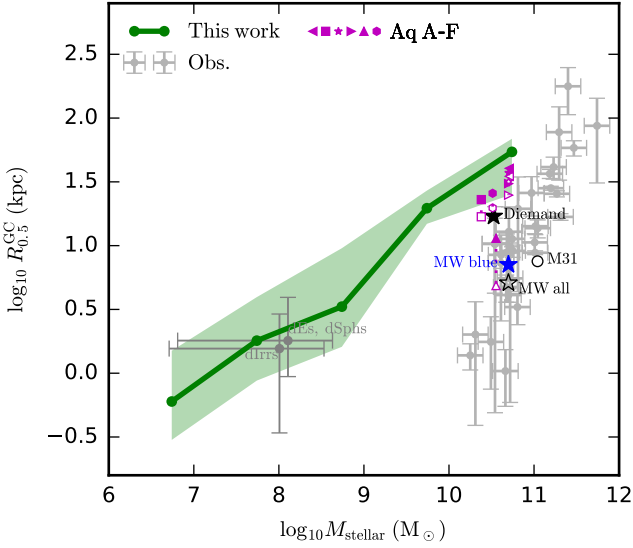


Figure A1. As for Fig. 4 but exploring the effects of adiabatic contraction. *Filled magenta symbols* indicate the Aquarius simulations without baryonic contraction, whilst *open symbols* are the median radii including the effect of a $10^{11} M_{\odot}$ baryonic disk. *Filled black star* indicates the radius from [Diemand et al. \(2005\)](#). Observations (*grey points*) and model (*green*) as for Fig. 4.

where filled/open magenta symbols indicate the results without and with adiabatic contraction, respectively.

Noticeably in Fig. 4 the median GC radius from [Diemand et al. \(2005\)](#), which has been averaged over several galaxies, is more than 1 sigma more compact than our results. We believe that this arises due to the different tagging techniques: whereas we tag only the most-bound particle of a GC-hosting dark matter halo to trace their $z = 0$ position, Diemand et al. uses the distribution of *all* particles in candidate halos. The latter, as is equivalent to a mass-weighted average that is mostly tracing the main progenitor of a MW halo, instead of the many more accreted and smaller subhalos. As an estimate, a $10^{12} M_{\odot}$ halo at $z = 0$ can have a main progenitor with mass 10^{10} already at $z = 9$, dominant over the contribution from the other subhalos. Other causes for the difference include the cosmology and the unique formation history of each galaxy.

Another work that has found more compatible (compact) predicted GC radii is [Griffen et al. \(2010\)](#), for a set of GCs for the Milky-Way analogue Aquarius A-2. This required the use of a relatively high reionization redshift for the MW ($z \approx 13$), and so the GCs are more clustered. We tested our method on the Aquarius ([Springel et al. 2008](#)) halos (these are of course a slightly different cosmology) and as see in Fig. A1 they fall, within the range of our distribution, with the exception of Aquarius E-4⁴. E-4 is the halo with the *least* tagged halos, which seems to be correlated with more compact distributions in our simulations.

A final test we made was to consider GC formation not only at the tagging redshift but prior redshifts as well,

comparable for example to [Griffen et al. \(2010\)](#). As such we ran an additional high time-resolution simulation down to redshift 8.65 in order to identify how many of our halos of mass above M_{tag} had in fact achieved this mass in more than one progenitor, however this only appeared to increase the number of halos by around 3%, and as such would make little difference to our result.

⁴ Usually one expects Aq-F to be the outlier since it experiences a late major merger, but surprisingly this not the case here.